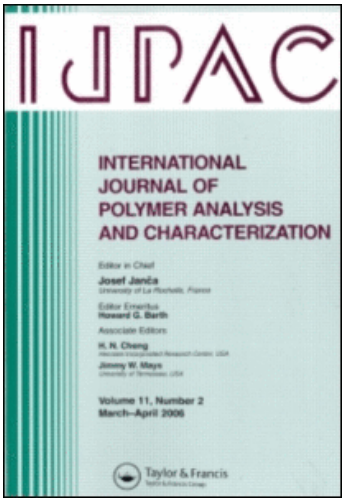

International Journal of Polymer Analysis and Characterization
Publication details, including instructions for authors and subscription information:
http://www.informaworld.com/smpp/title~content=t713646643

Characterization of the Microstructure of Biaxially Oriented Polypropylene Using Preparative Temperature-Rising Elution Fractionation

Yonggang Liu[a]; Shuqin Bo[a]
[a] State Key Laboratory of Polymer Physics and Chemistry,Changchun Institute of Applied Chemistry, Chinese Academy of Sciences, Changchun, China

Online publication date: 27 October 2010

To cite this Article Liu, Yonggang and Bo, Shuqin(2003) 'Characterization of the Microstructure of Biaxially Oriented Polypropylene Using Preparative Temperature-Rising Elution Fractionation', International Journal of Polymer Analysis and Characterization, 8: 4, 225 — 243
To link to this Article: DOI: 10.1080/10236660304880
URL: http://dx.doi.org/10.1080/10236660304880

International Journal of Polymer Anal. Charact., 8: 225–243, 2003

ISSN: 1023-666X print
DOI: 10.1080/110236660390198420

Taylor & Francis
Taylor & Francis Group

Characterization of the Microstructure of Biaxially Oriented Polypropylene Using Preparative Temperature-Rising Elution Fractionation

Yonggang Liu and Shuqin Bo
State Key Laboratory of Polymer Physics and Chemistry, Changchun Institute of Applied Chemistry, Chinese Academy of Sciences, Changchun, China

Two commercial biaxially oriented polypropylene (BOPP) resins, resin A and resin B, having different processing properties, were fractionated by preparative temperature-rising elution fractionation (TREF). The TREF fractions were further characterized by gel permeation chromatography (GPC), gel permeation chromatography coupled with light scattering (GPC-LS), wide-angle X-ray diffraction (WAXD), and differential scanning calorimetry (DSC). GPC-LS did not find visible long-chain branching in either resin A or B. The results from TREF and DSC indicate that the fractional melting parameter f(T) may be used to predict the profile of the TREF cumulative weight distribution curve. GPC results show that the molecular weights of the fractions tend to increase with elution temperature. WAXD and DSC data show that the crystallinity of fractions does not increase monotonically with increase of

Received 26 September 2001; accepted 11 January 2002.

This work was subsidized by the Special Funds for Major State Research Projects of China and supported by the State Key Laboratory of Polymer Physics and Chemistry. We thank Prof. Jinliang Qiao and Mr. Jingchun Zhang at the Beijing Research Institute of Chemical Industry for their assistance in performing parts of the TREF experiments. We are grateful to Dr. Eric T. Hsieh at Chevron Phillips Chemical Company for helpful discussions.

Address correspondence to Shuqin Bo, State Key Laboratory of Polymer Physics and Chemistry, Changchun Institute of Applied Chemistry, Chinese Academy of Sciences, Changchun 130022, China. E-mail:sqbo@ns.ciac.jl.cn

elution temperature. There appears to be a maximum in the plot of crystallinity versus elution temperature. The high-speed BOPP resin A has a lower isotacticity but a homogeneous isotacticity distribution and a higher molecular weight but a broader molecular weight distribution than resin B.

Keywords: Polypropylene; Microstructure; TREF; GPC; WAXD; DSC

INTRODUCTION

Biaxially oriented polypropylene (BOPP) film, which is widely used as a packaging material, is made of isotactic polypropylene (PP) resin. It is well known that so-called "isotactic" PP exhibits heterogeneity in isotacticity as well as molecular weight[1]. In isotactic PP, tacticity is a critical factor influencing its crystallinity and subsequent processability and final properties. However, the properties of heterogeneous polymers cannot be uniquely determined by average values of the parameters of chain microstructure. Hence, understanding the distribution of isotacticity in addition to molecular weight of PP is necessary in order to elucidate the relationship between its microstructure and properties[2].

Fractionation of PP according to molecular weight and isotacticity seems to be the best way to characterize the microstructure of PP. Gel permeation chromatography (GPC) has long been used to determine the molecular weight and molecular weight distribution (MWD) of polymers. Preparative temperature-rising elution fractionation (TREF), a technique that fractionates semicrystalline polymers according to their solubility-temperature relationship, has been widely used for the characterization of PP with respect to isotacticity[2].

In this article, two BOPP resins (resin A and resin B) having similar average molecular weights and isotacticities but differing in processing properties (resin A can be processed well at high-speed orientation during the processing of BOPP film, while resin B tends to break at the same processing conditions) were fractionated by preparative TREF. The microstructure of these two resins and their TREF fractions were studied by means of GPC, GPC coupled with light scattering (GPC-LS), wide-angle X-ray diffraction (WAXD), and differential scanning calorimetry (DSC). Based on the comparison between these two PP resins, the distributions in both molecular weight and isotacticity of BOPP are correlated to processing properties.

EXPERIMENTAL

Materials

Two commercial BOPP resins used in this study were kindly provided by China Petrochemical Corporation and coded as resin A and resin B. Resin A is a propylene/ethylene copolymer containing 0.32 wt% ethylene, determined by ^{13}C-NMR. Resin B is a homo-PP. ^{13}C-NMR results have shown that the two resins have similar isotacticity (resin A, %[m] = 94.2 and resin B, %[m] = 94.9). However, resin A can be processed well at high-speed orientation during the processing of BOPP film, while resin B tends to break at the same processing conditions.

Preparative TREF

Preparative TREF equipment used in this work is similar to that described in the literature[3]. In TREF experiments of PP, the solvent commonly used was 1,2,4-trichlorobenzene (TCB) or xylene. However, the high melting point of TCB (17°C) makes it tend to freeze when the room temperature is low; furthermore, it is hard to remove residual TCB from fractions. The boiling point of xylene is close to the highest elution temperature employed (140°C). Here, we use 1,2,4-trimethylbenzene (TMB) as the extracting solvent, which has a feasible melting point and boiling point and is volatilizable. A stainless steel column (5.0 cm diameter × 150 cm length), packed with 60–80 mesh glass beads, was loaded with about 10–15 g polymer samples dissolved in 700 mL TMB at 140°C. 2,6-Di-*tert*-butyl-4-methylphenol (BHT, 0.1% w/v) was added to TMB as an antioxidant in order to prevent thermal degradation of the polymer samples during fractionation. The column was then cooled to room temperature with a cooling program. The column temperature was decreased linearly from 140°C to 89°C in 15 h, reheated quickly to 107°C after being maintained at 89°C for 5 h, then cooled linearly from 107°C to 33°C in 55 h after being maintained at 107°C for 5 h. The fractionation procedure then was performed by increasing temperature stepwise. Extraction took place over temperatures ranging from 100° to 140°C divided into seven steps (110, 116, 118, 120, 122, 125, and 140°C for resin A and 100, 110, 116, 118, 120, 125, and 140°C for resin B). During each step, the column content was allowed to equilibrate at the set temperature overnight before it was eluted twice with 1000 mL of TMB. The eluted solution was cooled, precipitated with twice the volume of acetone, and filtered. The obtained polymer fractions were then dried in a vacuum oven below 60°C.

Characterization of TREF Fractions

Gel Permeation Chromatography

The molecular weight and MWD of the whole samples and the TREF fractions were determined at 150°C by a high-temperature gel permeation chromatograph (PL-GPC 220, Polymer Laboratories Ltd.). The columns used were three PLgel 10 μm Mixed-B type columns (300 × 7.5 mm). The eluent was TCB stabilized with BHT (0.05% w/v). The injection volume was 200 μL and the flow rate was 1.0 mL/min. Calibration was made by polystyrene standard EasiCal PS-1 (PL Ltd.). Universal calibration was applied to obtain the molecular weight of PP. The Mark-Houwink coefficients, K and α, used were 1.75×10^{-2} mL/g and 0.67 for polystyrene[4] and 1.90×10^{-2} mL/g and 0.725 for PP[5], respectively.

All sample solutions were prepared at 150°C with a PL-SP 260 high temperature sample preparation system (PL Ltd.). The sample concentration was about 0.2% (w/v) in eluent. The sample solutions were kept at 150°C for 2–4 h. The whole sample solutions were filtered before GPC experiments.

Gel Permeation Chromatography Coupled with Light Scattering

A PL-GPC 220 chromatograph coupled with an online PD2040 type two-angle light-scattering detector (Precision Detectors Inc., Bellingham, USA) was used for branching analysis of BOPP whole samples. The columns used were three PLgel 10 μm Mixed-B LS type columns (300 × 7.5 mm). The run conditions were the same as those for the GPC experiments. The PD2040 detector, which contained a 100 mW semiconductor diode laser (800 nm) and two detection angles (15° and 90°), was positioned before the refractive index detector. Calibration was made using narrow polyethylene standards (PL Ltd.). We used a value of −0.109 for dn/dc of polyethylene. The double logarithm relationship between radius of gyration and molecular weight was obtained, and branching analysis was made based on this relationship[6].

For linear flexible chains in dilute solution, the Flory-Fox equation is given by[7]

$$[\eta] = 6^{\frac{3}{2}}\phi R_g{}^3/M \tag{1}$$

where $[\eta]$, ϕ, R_g, and M are the intrinsic viscosity, universal constant (2.1×10^{23} mol^{-1}), radius of gyration, and molecular weight, respectively. The Mark-Houwink equation for PP in TCB at 135°C is[5]

$$[\eta] = 0.0190 \times \mathrm{M}^{0.725} \tag{2}$$

The combination of these two equations relates the radius of gyration with the molecular weight for linear PP in TCB at 135°C by

$$R_g = 0.0183 \times M^{0.575} \quad (3)$$

Equation (3) predicts the theoretical relationship between radius of gyration and molecular weight for linear PP in TCB at 135°C. Branching analysis can be made by comparing this theoretical relationship with the experimental relationship of BOPP whole samples.

The preparation method of sample solutions was the same as that of the above GPC experiments, except that the eluent used here was first filtered with a 0.2 μm pore size membrane.

Wide-Angle X-Ray Diffraction

WAXD experiments were carried out on powered samples at ambient temperature using a Rigaku D/max 2500 V PC X-ray diffractometer. Nickel-filtered Cukα_1 X-rays with a wavelength of 0.154056 nm generated at 40 kV and 200 mA were employed. Scattered intensities were measured as a function of 2θ values between 5° and 50° in steps of 0.02°.

The X-ray crystallinity $W_{c,x}$ was calculated from

$$W_{c,x} = I_c/(I_c + KI_a) \quad (4)$$

where I_c represents the integrated area of crystalline diffraction peaks, I_a is a corresponding portion of the amorphous halo, and K is a correction factor. $W_{c,x}$ was calculated by assuming $K = 1$.

Differential Scanning Calorimetry

DSC scans were recorded on a Perkin-Elmer DSC-7 calorimeter. The samples (about 4–5 mg) were first heated from 50° to 200°C at a rate of 10°C/min, held at 200°C for 3 min to remove thermal history, then cooled from 200° to 50°C at 10°C/min, held at 50°C for 1 min, and finally heated again to 200°C at 10°C/min. Temperature calibration was performed using indium. Crystallization temperature T_c and heat of crystallization ΔH_c, melting temperature T_m, and heat of fusion ΔH_m were measured during cooling and reheating experiments, respectively.

The calorimetric crystallinity $W_{c,h}$ was calculated from

$$W_{c,h} = \Delta H_m/\Delta H_m^0 \quad (5)$$

where ΔH_m is the heat of fusion of a semicrystalline PP and ΔH_m^0 is that of a 100% crystalline PP sample. $W_{c,h}$ was calculated by assuming $\Delta H_m{}^0 = 138\,J/g$[8].

A fractional melting parameter f(T), which is the percentage of the total DSC endotherm area that is melted at a temperature T, is derived from the reheat DSC scan. An empirical temperature dependent crystallinity index $[(1 - f)\Delta H_m/\Delta H_m{}^0]$ was calculated[9].

RESULTS AND DISCUSSION

Characterization of the Whole Samples

The molecular weight and MWD of resins A and B are summarized in Table I. Figure 1 shows the differential MWD and cumulative MWD curves of resins A and B. These results indicate that resin A has a higher molecular weight and a broader MWD than resin B. It is generally accepted that a broad MWD helps to improve processibility.

The double logarithm relationships between radius of gyration and molecular weight of resins A and B, as well as the theoretical relationship for linear PP, are plotted in Figure 2. Although the experimental curves of resins A and B deviate slightly from the predicted curve of linear PP, they still have a linear relationship, indicating there is no long-chain branching in these samples. Thus, the difference in processing properties for resins A and B is not a result of long-chain branching.

Table II presents the DSC results for resins A and B. A higher T_m and a higher ΔH_m are observed for resin B in comparison to resin A. Figure 3

TABLE I Molecular weight and MWD of resins A and B

Sample	M_w(k)	M_n(k)	M_w/M_n
Resin A	389	57.4	6.78
Resin B	341	73.1	4.66

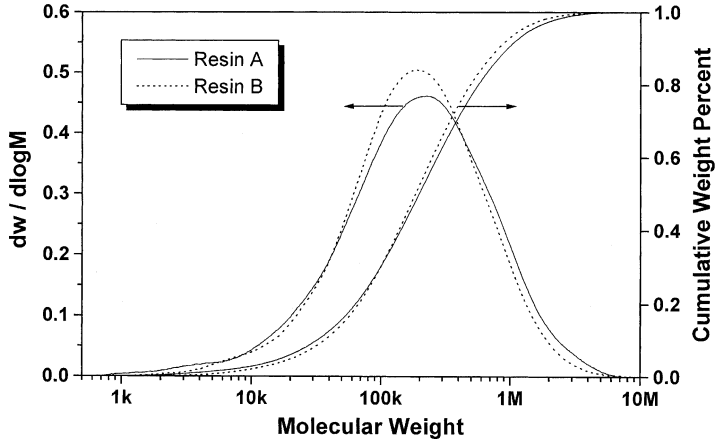

FIGURE 1 Differential MWD and cumulative MWD curves of resins A and B.

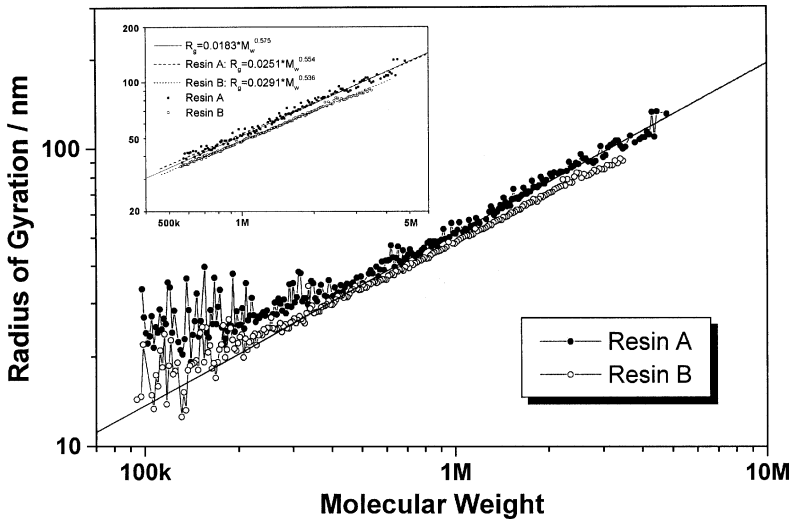

FIGURE 2 Double logarithm relationships between radius of gyration and molecular weight of resins A and B (the straight line is the theoretical relationship for linear PP).

TABLE II Thermal properties of resins A and B

Sample	T_c (°C)	T_m (°C)	ΔH_c (J/g)	ΔH_m (J/g)
Resin A	111.6	159.2	93.3	92.3
Resin B	111.1	161.2	96.2	94.2

shows the fractional melting parameter f(T) derived from the reheat DSC scans for resins A and B. The f(T) curve of resin B shifts to a higher temperature region in comparison to resin A. These results indicate a higher crystallizability and a higher crystallinity for resin B than resin A, as a result of the higher isotacticity of resin B. In addition, a small amount of comonomer (0.32 wt% ethylene) in resin A disrupted the isotactic sequences, and thus lowered the crystallizability of the chains. Figure 4 shows the empirical crystallinity index for resins A and B. It can be seen that resin B has a higher crystallinity index at the same temperature in comparison to that of resin A. Thus, a slight decrease in isotacticity and a small amount of comonomer existing in the resin reduced crystallinity and softened the resin, which are favorable properties for the processibility of BOPP film.

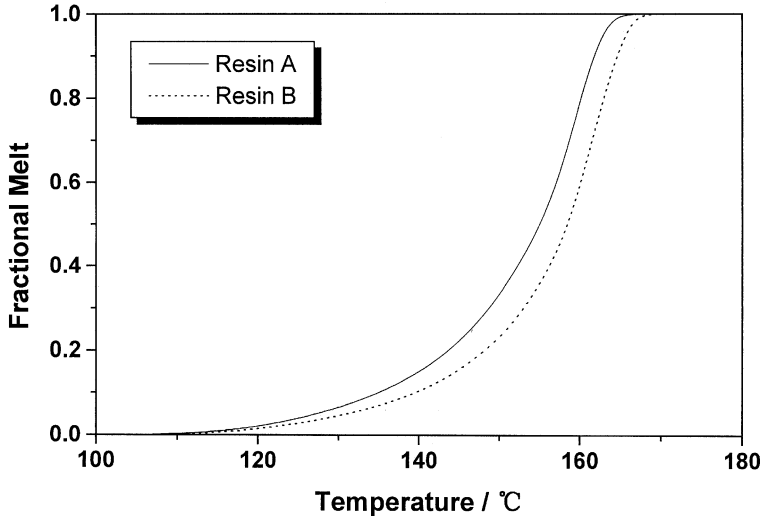

FIGURE 3 The fractional melting parameter f(T) derived from reheat DSC scans for resins A and B.

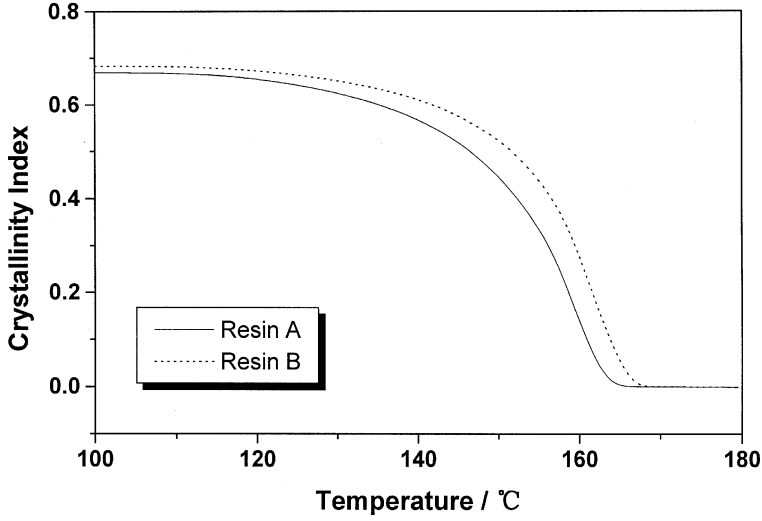

FIGURE 4 The crystallinity index parameter derived from reheat DSC scans for resins A and B.

However, analysis from only the above-mentioned average values of microstructure is not sufficient to completely explain processing properties. Information concerning the microstructure distribution of BOPP resin is necessary in order to elucidate the relationship between its microstructure and processing properties. This kind of information can be obtained via TREF and subsequent characterization of TREF fractions by GPC, WAXD, and DSC.

TREF

The total recoveries of TREF fractionations were 100.2% and 97.4% for resins A and B, respectively. The fractionation data of resins A and B are summarized in Table III. The weight fraction (w_i%) and cumulative weight fraction (Σw_i%) as a function of elution temperature for resins A and B are shown in Figures 5 and 6, respectively.

It is clear that 57.6% of resin A was eluted at a lower temperature of 116°C, and the amount of fractions eluted at 110° and 116°C added up to 90.6% of the whole sample weight, while 60.0% of resin B was eluted at a higher temperature of 125°C. The results indicate that resin A has a lower isotacticity and a more homogeneous isotacticity distribution than resin B, because TREF fractionates PP mainly based on isotacticity[10]. These data are in good agreement with the results of DSC and ^{13}C-NMR for the whole samples. ^{13}C-NMR on the fractions will be studied further.

A comparison of Figures 3 and 6 shows that the fractional melting parameter f(T) curves have similar shape with the TREF cumulative weight distribution curves, and both f(T) and TREF cumulative weight distribution curves of resin B shift to a higher temperature region in comparison to resin A. Thus, the fractional melting parameter f(T) may

TABLE III TREF data of resins A and B

Elution temperature (°C)	Resin A		Resin B	
	w_i%	Σw_i %	w_i%	Σw_i %
100	—	—	9.7	9.7
110	33.0	33.0	10.7	20.4
116	57.6	90.6	13.2	33.6
118	3.63	94.2	2.26	35.8
120	2.47	96.7	3.97	39.8
122	1.03	97.7	—	—
125	0.91	98.6	60.0	99.8
140	1.37	100.0	0.17	100.0

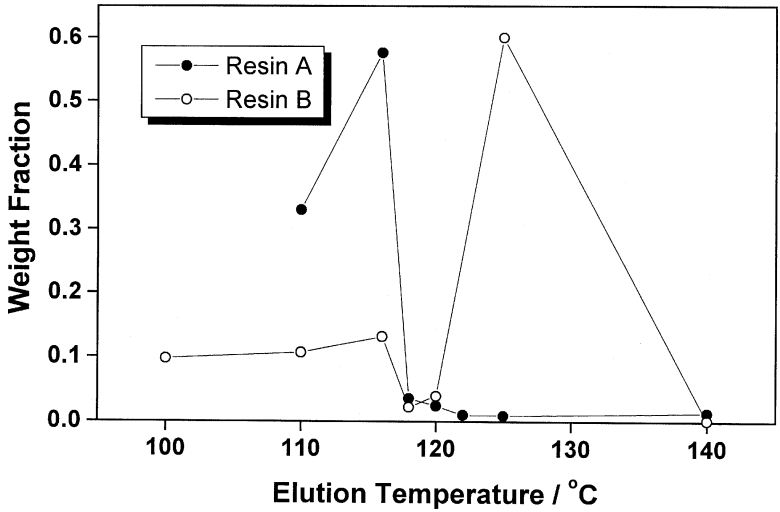

FIGURE 5 Weight fraction as a function of elution temperature for resins A and B.

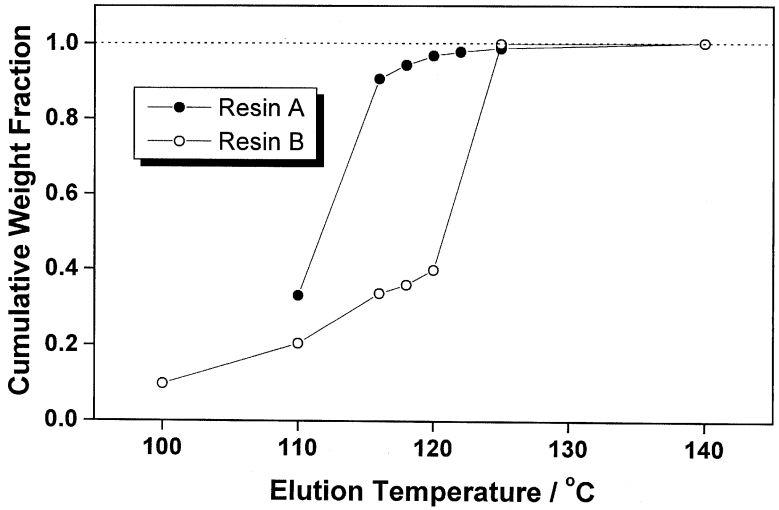

FIGURE 6 Cumulative weight fraction as a function of elution temperature for resins A and B.

be used to predict the profile of the TREF cumulative weight distribution curves when it is applied to new resins.

GPC Analysis Of TREF Fractions

Table IV summarizes the values of the molecular weight and MWD of the TREF fractions. The MWD curves of resin B as well as its TREF fractions are profiled in Figure 7. The area under each MWD curve is made proportional to the relative weight percent of the corresponding fraction in the whole sample. A summation MWD curve, which is the sum of the MWD curves of the fractions, is obtained. The molecular weight and MWD of the "summation sample" are also calculated and are in good agreement with those of the whole sample. It suggests that TREF is an efficient fractionation method and there is no degradation during the fractionation.

The M_w as a function of elution temperature for resin A and resin B is shown in Figure 8. It is found that the molecular weights of the fractions tend to increase with elution temperature. Xu et al.[10,11] and Kioka et al.[12] had also found a molecular weight increase of fractions with elution temperature and considered it due to the coincidence of molecular weight and isotacticity. However, this trend reflects intermolecular isotactic heterogeneity of different molecular weight PP. The low molecular weight fractions contain more stereo-defects since they elute at low elution temperature, while the high molecular weight fractions, which elute at higher elution temperature, have longer isotactic sequences. It can also be observed that at the same elution temperature, fractions of resin A have a higher molecular weight than that of resin B. This result indicates that shorter chains of resin

TABLE IV Molecular weight and MWD for TREF fractions of resins A and B

Elution temperature (°C)	Resin A			Resin B		
	M_w(k)	M_n(k)	M_w/M_n	M_w(k)	M_n(k)	M_w/M_n
100	—	—	—	85.5	17.2	4.98
110	132	26.2	5.02	98.1	40.8	2.41
116	433	152	2.86	128	61.6	2.08
118	497	173	2.88	134	68.0	1.97
120	572	200	2.86	161	85.3	1.89
122	767	316	2.42	—	—	—
125	822	323	2.54	490	211	2.32
140	1298	463	2.80	—	—	—
Summation	358	59.5	6.02	340	71.7	4.74

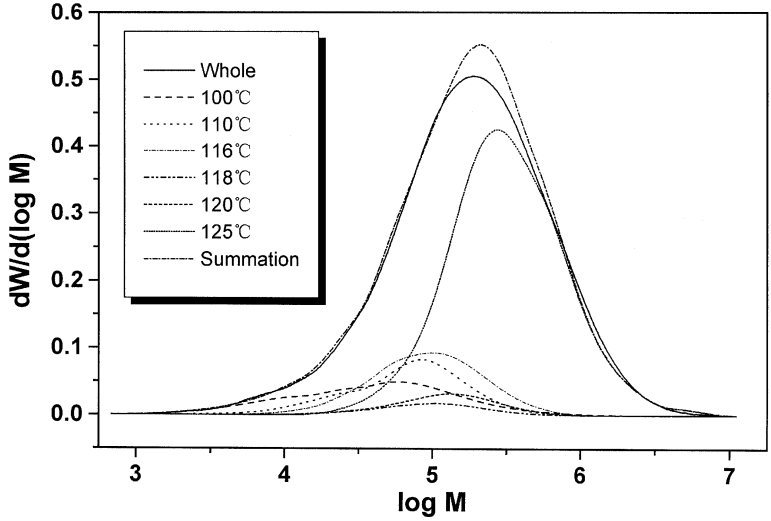

FIGURE 7 MWD profiles of resin B whole sample and its TREF fractions.

B have the same crystallizability as longer chains of resin A, reflecting different interchain isotactic heterogeneity of resins A and B. Viville et al.[13] had also found this molecular-weight-dependent interchain isotactic heterogeneity for highly isotactic PP.

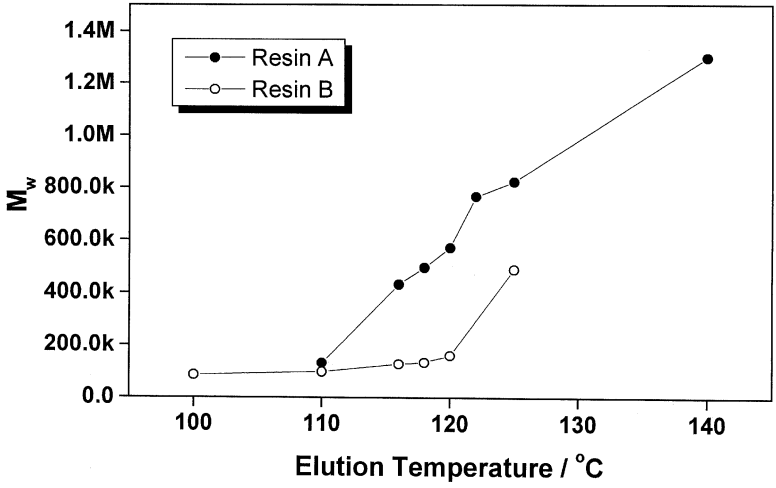

FIGURE 8 M_w as a function of elution temperature for resins A and B.

WAXD and DSC Analysis of TREF Fractions

Table V summarizes the values of T_c, T_m, ΔH_c, ΔH_m, $W_{c,h}$, and $W_{c,x}$ for TREF fractions of resins A and B. Figure 9 shows WAXD diffractographs of TREF fractions of resin A. It can be seen that the characteristic peaks of α-PP at $2\theta = 14.12^\circ$, 17.02°, 18.57°, 21.05°, and 21.89° represent the (110), (040), (130), (111), (131), and (041) diffraction planes. The WAXD diffractographs of TREF fractions of resin B are similar to those of resin A except that the fraction eluted at 100°C for resin B shows a larger amorphous halo than the others, indicating more amorphous component in this fraction.

Figure 10 shows the DSC endotherms of TREF fractions of resin B. It can be seen that the endotherm peaks of the fractions move toward a higher temperature with increasing elution temperature. The fractional melting parameter f(T) curves (Figure 11) of TREF fractions of resin B also shift to a higher temperature region with increasing elution temperature. These results indicate an increase of isotacticity and length of isotactic sequences with increasing elution temperature. The experimental results of DSC (endotherm peak and f[T]) of TREF fractions of resin A are identical with those of resin B. Figure 12 shows the f(T) curves for TREF fractions of resins A and B eluted at 110°C. It can be observed that at the same elution temperature, the f(T) curve of resin B fractions shifts to a higher temperature region, indicating a higher crystallinity for resin B fractions, owing to its higher isotacticity. It can also be observed

TABLE V T_c, T_m, ΔH_c , ΔH_m, $W_{c,h}$, and $W_{c,x}$ for TREF fractions of resins A and B

Sample	Elution temperature (°C)	T_c (°C)	T_m (°C)	ΔH_c (J/g)	ΔH_m (J/g)	$W_{c,h}$	$W_{c,x}$
Resin A	110	109.0	151.4/158.7	84.1	75.5	54.72	58.75
	116	109.4	162.3	93.8	88.4	64.03	62.58
	118	114.6	161.1	94.9	91.8	66.54	58.26
	120	113.8	161.1	96.1	91.5	66.31	62.36
	122	115.3	161.3	84.5	81.4	58.95	57.53
	125	115.1	160.8	85.2	86.2	62.43	59.41
	140	115.5	163.7	88.3	83.0	60.14	57.80
Resin B	100	95.2	131.3/140.5	40.1	31.0	22.48	37.49
	110	111.7	155.5/163.1	96.2	99.1	71.82	61.04
	116	112.8	158.7	101.7	104.5	75.75	—
	118	114.0	159.4	100.8	104.7	75.90	62.08
	120	114.0	161.2	100.5	100.7	72.94	65.32
	125	110.4	164.4	99.1	93.6	67.80	61.98

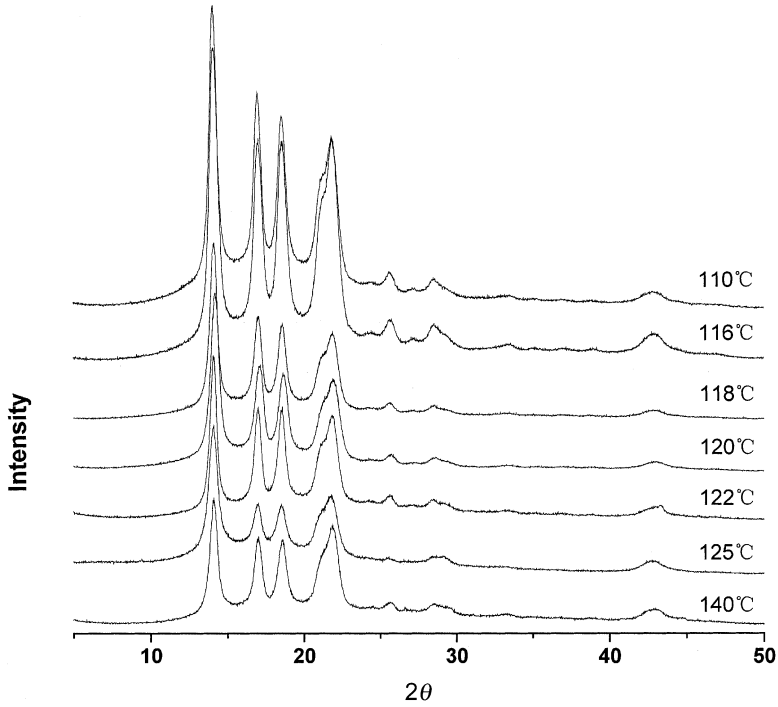

FIGURE 9 WAXD diffractograms of TREF fractions of resin A.

that the f(T) curves of TREF fractions cover a broader temperature region for resin B than that for resin A, indicating that the interchain distribution of isotactic sequence lengths is more heterogeneous for resin B than that for resin A.

The crystallinity data in Table V confirm these conclusions. Figures 13 and 14 show the relationships between X-ray crystallinity $W_{c,x}$, calorimetric crystallinity $W_{c,h}$, and elution temperature for TREF fractions of resins A and B, respectively. Resin B fractions show a higher crystallinity than resin A fractions at the same elution temperature, resulting from a longer isotactic sequence for resin B fractions. Furthermore, the crystallinity of TREF fractions does not increase monotonically with increase of elution temperature. There appears to be a maximum in the plot of crystallinity versus elution temperature (Figures 13 and 14). The lower crystallinity of fractions eluted at lower temperatures is due to the presence of more amorphous components. The crystallinity of fractions increases with increasing elution temperature below 120°C. At elution temperatures above 120°C, the

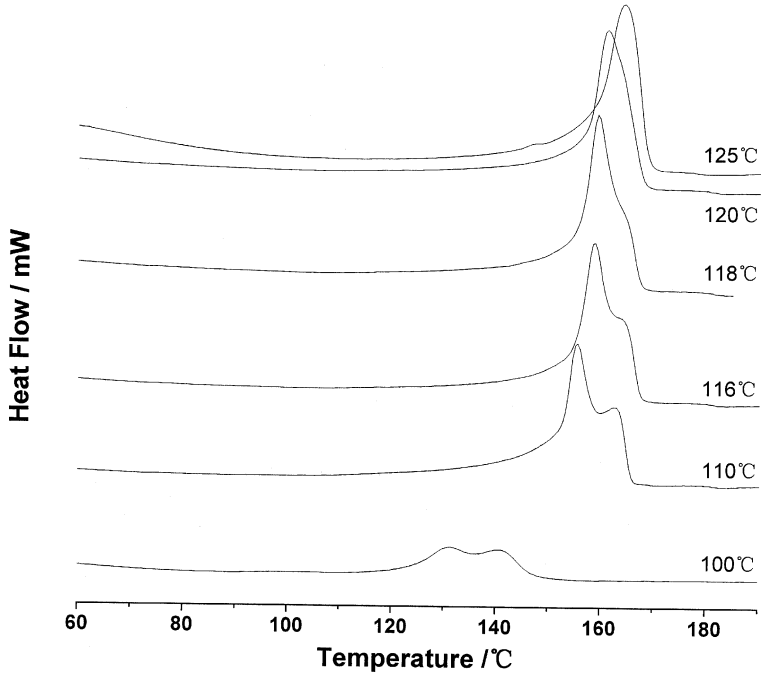

FIGURE 10 DSC endotherms of TREF fractions of resin B.

isotacticity of fractions increased little (because the endotherm peak of the fractions changed only slightly to higher temperature), but the molecular weight of fractions increased drastically. The decrease of crystallinity for these high molecular weight fractions can be a result of the imperfection of crystallization due to restricted mobility of very long chains in these fractions.

Although it is generally accepted that TREF fractionates semi-crystalline polymers according to crystallinity[2], there have been suggestions that TREF separates macromolecules according to both crystallinity and the longest crystallizable sequences[13–16]. As for BOPP, the crystallizable sequences are the isotactic sequences. Further studies on the TREF fractions by ^{13}C-NMR will provide direct proofs.

CONCLUSIONS

Two commercial BOPP resins having different processing property were fractionated by preparative TREF, and the TREF fractions were

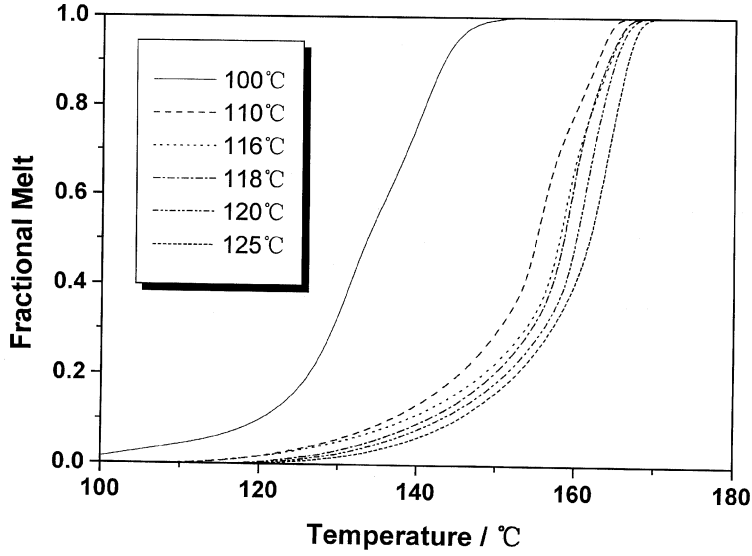

FIGURE 11 The fractional melting parameter f(T) derived from reheat DSC scans for TREF fractions of resin B.

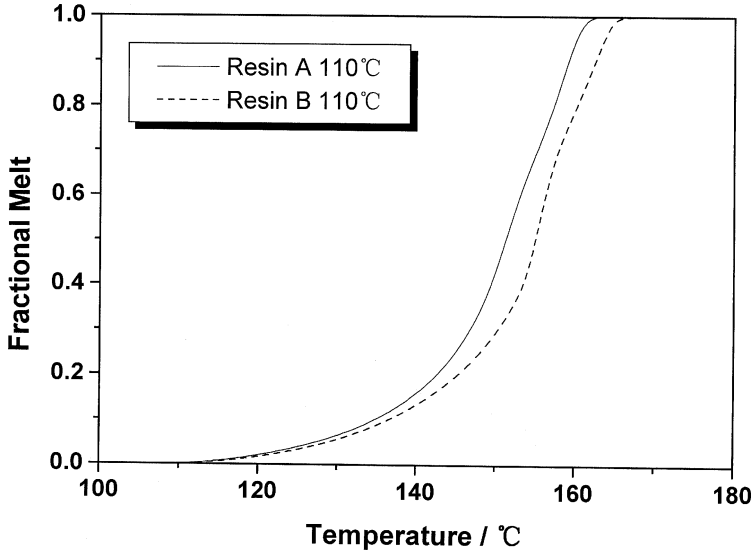

FIGURE 12 The fractional melting parameter f(T) derived from reheat DSC scans for TREF fractions of resins A and B eluted at 110°C.

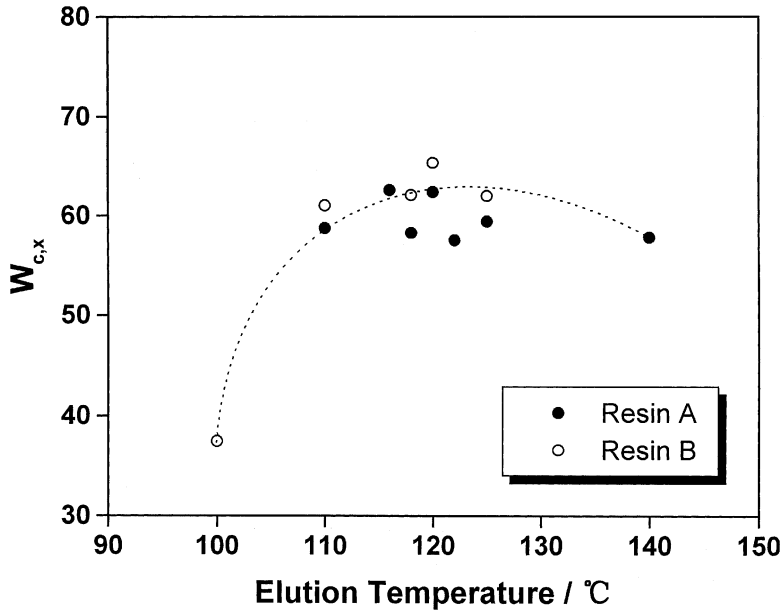

FIGURE 13 The relationships between X-ray crystallinity and elution temperature for TREF fractions of resins A and B.

further characterized by GPC, GPC-LS, WAXD, and DSC. GPC-LS did not indicate long-chain branching in resins A and B. DSC results of the whole samples show a higher crystallinity resulting from its higher isotacticity for resin B than that for resin A. The fractional melting parameter f(T) was derived from the reheat DSC scan. By comparing the f(T) and TREF cumulative weight distribution curves of both resins A and B, it is found that the f(T) curves have shapes similar to the TREF cumulative weight distribution curves and that both f(T) and TREF cumulative weight distribution curves of resin B shift to a higher temperature region in comparison to resin A. Thus, the fractional melting parameter f(T) may be used to predict the profile of the TREF cumulative weight distribution curves when it is applied to new resins.

The molecular weights of TREF fractions tend to increase with elution temperature, while the crystallinity of fractions does not increase monotonically with elution temperature. There appears to be a maximum in the plot of crystallinity versus elution temperature, indicating the fractionation is based on both crystallinity and the longest crystallizable sequences in a chain. TREF combined with other analysis methods provides detailed information about isotacticity and molecular weight heterogeneity of

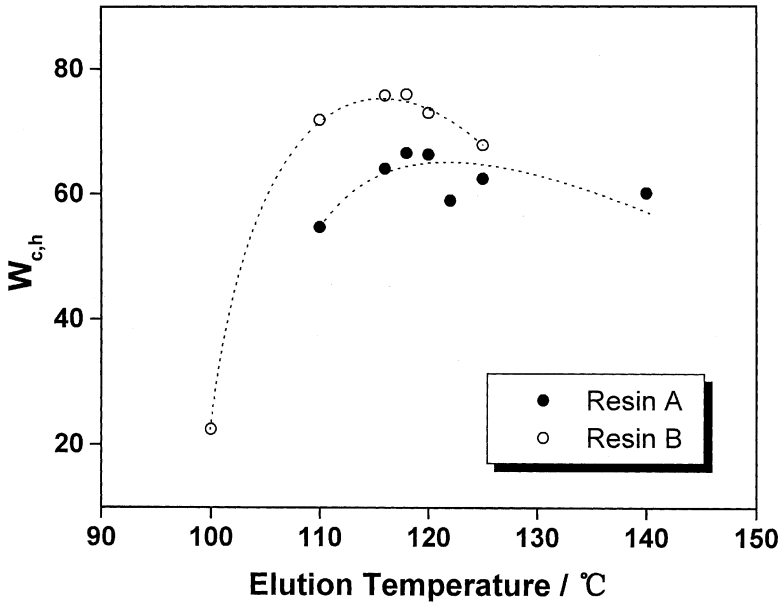

FIGURE 14 The relationships between calorimetric crystallinity and elution temperature for TREF fractions of resins A and B.

different PP. It is found that the high-speed BOPP resin A has a lower isotacticity but a more homogeneous isotacticity distribution and a higher molecular weight but a broader MWD than resin B.

REFERENCES

[1] Kamath, P. M., and Wild, L. (1966). *Polym Eng Sci.* **6**, 213–216.
[2] Soares, J. B. P., and Hamielec, A. E. (1995). *Polymer*. **36**, 1639–1654.
[3] Hsieh, E. T., Tso, C. C., Byers, J. D., Johnson, T. W., Fu, Q., and Cheng, S. Z. D. (1997). *J. Macromol. Sci. Phys*. **B36**, 615–628.
[4] Kurata, M. and Tsunashima, Y. (1999). In vol. VII *Polymer Handbook, 4th ed.*, J. Brandrup, E. H. Immergut, and E. A. Grulke, eds., Wiley Interscience, New York: 1–83.
[5] Scholte, Th. G., Meijerink, N. L. J., Schoffeleers, H. M., and Brands, A. M. G. (1984). *J. Appl. Polym. Sci.* **29**, 3763–3782.
[6] Havard, T. and Wallace, P. (1999). Factors affecting molecular weight and branching analysis of metallocene catalyzed polyolefins using on-line GPC with light scattering, and viscometry detection. In: *Chromatography of Polymers: Hyphenated and Multi-dimensional Techniques*, T. Provder, ed., American Chemical Society, Washington, DC.: 232–248.
[7] Flory, P. J. and Fox, T. G. (1951). *J. Am. Chem. Soc*. **73**, 1904–1908.
[8] Yuksekkalayci, C., Yilmazer, U., and Orbey, N. (1999). *Polym. Eng. Sci*. **39**, 1216–1222.

[9] Phillips, R. A., and Nguyen, T. (2001). *J. Appl. Polym. Sci.* **80**, 2400–2415.
[10] Xu, J., Feng, L., Yang, S., Yang, Y., and Kong, X. (1997a). *Macromolecules*. **30**, 7655–7660.
[11] Xu, J., Feng, L., Yang, S., Yang, Y., and Kong, X. (1997b). *Polym. J.* **29**, 713–717.
[12] Kioka, M., Makio, H., Mizuno, A., and Kashiwa, N. (1994). *Polymer*. **35**, 580–583.
[13] Viville, P., Daoust, D., Jonas, A. M., Nysten, B., Legras, R., Dupire, M., Michel, J., and Debras, G. (2001). *Polymer*. **42**, 1953–1967.
[14] Bonner, J. G., Frye, C. J., and Capaccio, G. (1993). *Polymer*. **34**, 3532–3534.
[15] Elicabe, G., Cordon, C., and Carella, J. (1996). *J. Polym. Sci. Part. B. Polym. Phys*. **34**, 1147–1154.
[16] Zhang, M., Lynch, D.T., and Wanke, S.E. (2000). *J. Appl. Polym. Sci*. **75**, 960–967.